Novel Radar Waveform Optimization for a Cooperative Radar-Communications System

ALEX RAJAN CHIRIYATH, Member, IEEE
Arizona State University, Tempe, AZ, USA

SHANKARACHARY RAGI, Member, IEEE
South Dakota School of Mines and Technology, Rapid City, SD, USA

HANS D. MITTELMANN
Arizona State University, Tempe, AZ, USA

DANIEL W. BLISS, Fellow, IEEE
Arizona State University, Tempe, AZ, USA

We develop and present a novel *minimum estimation error variance* waveform design method. The method optimizes the spectral shape of a unimodular radar waveform such that the performance of a joint radar-communications system that shares spectrum is maximized. We also develop the novel spectral water-filling successive interference cancelation data rate, which employs the continuous spectral water-filling algorithm to obtain the optimal communications power spectrum. We perform a numerical study to compare the performance of the new technique with the previously derived spectral mask shaping method. The global estimation rate and the data rate capture the radar and the communications performance, respectively.

Manuscript received February 26, 2018; revised December 4, 2018; released for publication March 24, 2019. Date of publication April 1, 2019; date of current version June 7, 2019.

DOI. No. 10.1109/TAES.2019.2908739

Refereeing of this contribution was handled by J. T. Curran.

The work of A. R. Chiriyath and D. W. Bliss was supported in part by the Office of Naval Research. The work of S. Ragi and H. D. Mittelmann was supported in part by Air Force Office of Scientific Research under Grant FA 9550-15-1-0351.

Authors' addresses: A. R. Chiriyath and D. W. Bliss are with the Bliss Laboratory of Information, Signals, and Systems and the Center for Wireless Information Systems and Computational Architectures, Arizona State University, Tempe, AZ 85281 USA, E-mail: (achiriya@asu.edu; d.w.bliss@asu.edu); S. Ragi is with the Department of Electrical and Computer Engineering, South Dakota School of Mines and Technology, Rapid City, SD 57701 USA, E-mail: (Shankarachary.Ragi@sdsmt.edu); H. D. Mittelmann is with the School of Mathematical and Statistical Sciences, Arizona State University, Tempe, AZ 85287 USA, E-mail: (mittelmann@asu.edu). *(Corresponding author: Alex Rajan Chiriyath.)*

I. INTRODUCTION

Spectral congestion is quickly becoming a problem for the telecommunications sector [1] and cooperative spectrum sharing between radar and communications systems such that both systems mutually benefit from the presence of each other has been proposed as a potential solution [2], [3]. In order to determine how to efficiently share spectral resources and achieve radio frequency (RF) convergence [4], a thorough understanding of the fundamental performance limits of cooperative spectrum sharing is needed. Bliss *et al.* [3], [5] investigated the fundamental limits of an in-band cooperative radar and communications system and developed inner bounds on performance for such a system. However, these bounds were specifically developed by considering only local estimation errors using a radar waveform that is suboptimal for joint performance. Generalizing these performance bounds can help establish limits for cooperative spectrum sharing.

Furthermore, these joint radar-communications performance bounds were found to depend on the shape of the radar waveform spectrum [3], [5]. For a given bandwidth, an impulse-like radar spectral shape (small root mean square (rms) bandwidth) was found to be favorable for communications performance, whereas a radar waveform spectrum with more energy at the edges of the bandwidth allocation (large rms bandwidth) was found to be more favorable for estimation performance. However, the latter waveform also has higher autocorrelation side-lobes or ambiguity, which negatively impacts the global (local and nonlocal regime) estimation performance by increasing the radar threshold signal-to-noise ratio (SNR) at which nonlocal estimation errors occur. Thus, the shape of the radar spectrum poses a tradeoff both in terms of radar performance versus communications performance and in terms of improved estimation performance versus an increased radar threshold SNR.

Paul *et al.* [6] generalized the performance bounds developed by Bliss *et al.* [3], [5] by taking nonlocal estimation errors into account and tuning the shape of the radar waveform spectrum to maximize joint radar-communications performance. The results presented in this paper are an extension of the work presented by Paul *et al.* [6]. In this paper, we present a new radar waveform design method for a joint radar-communications system that optimizes the radar waveform spectrum to maximize radar performance or minimize estimation error variance in the nonlocal (or low-SNR) regime and optimizes the communications power spectrum to maximize communications performance by employing the continuous spectral water-filling algorithm [7]. This novel method designs a jointly optimal radar waveform that is constant modulus, unlike the method presented by Paul *et al.* [6]. The global estimation rate, introduced in [6], and data rate capture radar and communications performance, respectively. In order to place emphasis on waveform design approaches and their performance, we assume a simple scenario with a single target and no clutter. The problem scenario considered in this paper is given by Fig. 1.

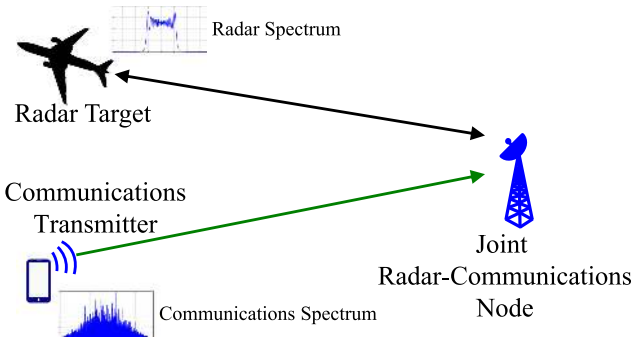

Fig. 1. Joint radar-communications system simulation scenario for radar waveform design. In this scenario, a radar and communications user attempt to use the same spectrum-space-time. This scenario is instructional, and can easily be scaled to more complicated scenarios by using it as a building block to construct real-world examples.

A. Contributions

The main contributions of this paper are summarized below.

1) Develop novel *minimum estimation error variance* waveform design method to design a constant modulus radar waveform that maximizes radar performance of a joint radar-communications system.
2) Develop novel spectral water-filling SIC data rate that maximizes communications performance of a joint radar-communications system.
3) Perform numerical study of the effects of radar threshold SNR and the order of nonlinear chirp phase on waveform design performance.
4) Compare performance of new waveform design algorithm with previously derived *spectral-mask shaping* waveform design method.

B. Background

The performance bounds presented in Bliss *et al.* [3]–[5], [8], which only considered local estimation errors, were shown to be dependent primarily on the rms bandwidth of the radar waveform. Paul *et al.* [6] extended the estimation rate to consider nonlocal or global estimation errors and employed a spectral mask to shape the radar waveform spectrum so as to maximize the performance of a joint radar-communications system. An evolutionary optimization algorithm was applied to find the optimal spectral mask that maximizes radar and communications performance (estimation and data rate, respectively) and new performance bounds were developed. Performance bounds comparing communications performance versus radar detection performance were derived for a joint radar-communications system in [9].

Modern approaches to the RF convergence problem have looked at waveform design in the context of a single, unified waveform for radar and communications. For example, orthogonal frequency-division multiplexing (OFDM) is commonly chosen for this dual waveform [10]–[14], where a single transmission is used for communications and monostatic radar. Most results using OFDM waveforms revealed data-dependent ambiguities, opposing cyclic prefix requirements, and demanding peak-to-average power ratio (PAPR) requirements. Spread spectrum waveforms have also been proposed for their autocorrelation properties [15]–[17], and multiple-input multiple-output (MIMO) radar techniques have been suggested, given that the independent transmitted waveforms allow more degrees of freedom for joint radar-communications codesign [18]–[20]. Multiple orthogonal linear frequency-modulated (FM) chirps have also been proposed to accomplish both radar detection and communications transmissions in a MIMO system [21]. Both systems have fundamentally different waveform requirements and that is why, contrary to the aforementioned approaches, the waveform design method proposed in this paper assumes that radar and communications systems transmit separate waveforms.

Researchers have also looked at optimization theory based radar waveform design methods that look to optimize radar performance, whereas the communications system is constrained to reduce interference. Optimization theory is used to maximize some radar performance metrics (detection probability, ambiguity function features, etc.) and keep interference to other in-band systems at a minimum [22]–[24] or impose constraints on the communications rate of other in-band systems [25].

Researchers have searched several other research areas for potential solutions to the spectral congestion problem. Some researchers looked at spatial mitigation as a means to improve spectral interoperability [26]–[28]. Joint coding techniques, such as robust codes for communications that have desirable radar ambiguity properties, as well as codes that trade data rate and channel estimation error have been investigated as codesign solutions [29]–[32].

C. Problem Set-Up

We consider the scenario shown in Fig. 1, which involves a radar and communications user attempting to use the same spectrum-space-time. We consider the joint radar-communications receiver to be a radar transmitter/receiver that can act as a communications receiver. The key assumptions made in this paper for the scenario described in Fig. 1 are as follows.

1) Joint radar-communications receiver is capable of simultaneously decoding a communications signal and estimating a target parameter.
2) Radar detection and track acquisition have already taken place.
3) Radar system is an active, single-input single-output (SISO), monostatic, and pulsed system.
4) Interpulse ambiguities between radar pulses not considered.
5) A single SISO communications transmitter is present.
6) Only one radar target is present.
7) Target range or delay is the only parameter of interest.
8) Target cross section is well estimated.

TABLE I
Survey of Notation

Variable	Description
$\langle\cdot\rangle$	Expectation
$\|\cdot\|$	L2-norm or absolute value
$Q_M(.)$	Marcum Q-function
$\delta(.)$	Dirac-delta function
f	Frequency
t	Time
B	Full bandwidth of the system
B_{rms}	Root-mean-squared radar bandwidth
$x(t)$	Unit-variance transmitted radar signal
$X(f)$	Radar signal frequency response
P_{rad}	Radar power
τ	Time delay to target
a	Target complex combined antenna, cross-section, and propagation gain
T	Radar pulse duration
δ	Radar duty factor
P_{com}	Total communications power
b	Complex combined antenna gain and communications propagation loss
$n(t)$	Receiver thermal noise
$n_{\text{resi}}(t)$	Post-SIC radar residual
σ^2_{noise}	Thermal noise power
k_B	Boltzmann constant
T_{temp}	Absolute temperature
$\sigma^2_{\tau,\text{proc}}$	Variance of range fluctuation process
σ^2_{CRLB}	Cramèr-Rao lower bound or estimation error variance
ISNR	Integrated radar SNR
$p_1,\ldots,p_N$	Phase parameters of polynomial chirp

It should be noted that the performance bounds and results presented in this paper are very closely dependent on the employed receiver model. By employing a mitigation technique called successive interference cancelation (SIC) (discussed later in the paper) at the receiver, the communications data rate at the receiver becomes dependent on the radar waveform spectrum [5]. Employing different mitigation techniques and changing the receiver model will result in a set of performance bounds that are different from the ones presented in this paper.

II. JOINT RADAR-COMMUNICATIONS SYSTEM—RECEIVER MODEL AND PERFORMANCE METRICS

In this section, we present both the model used to represent the joint radar-communications receiver and the performance metrics used in this paper to characterize radar and communications performance for the joint radar-communications system. A discussion of the SIC mitigation techniques employed at the receiver is also provided. We present a table of significant notation that is employed in this paper in Table I.

A. SIC Receiver Model

We present the joint radar-communications receiver model that employs SIC, an interference mitigation technique. It is this receiver model that causes communications performance to be closely tied to the spectrum of the radar waveform. This receiver model was first developed in [3].

We assume that we have some knowledge of the radar target range (or time-delay), based on previous observations, up to some random fluctuation or process noise, which is modeled as a zero-mean random variable $n_{\tau,\text{proc}}(t)$.

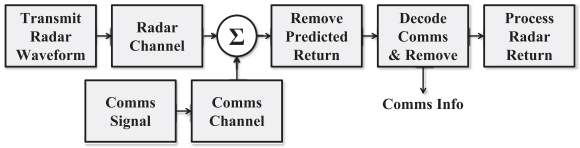

Fig. 2. Joint radar-communications system block diagram for SIC scenario. The radar and communications signals have two effective channels, but arrive converged at the joint receiver. The radar signal is predicted and removed, allowing a reduced rate communications user to operate. Assuming near perfect decoding of the communications user, the ideal signal can be reconstructed and subtracted from the original waveform, allowing for unimpeded radar access.

Using this information, we can generate a predicted radar return and subtract it from the joint radar-communications received signal. Since there is some error in the predicted and actual target locations, this predicted radar signal suppression leaves behind a residual contribution, $n_{\text{resi}}(t)$, to the joint received signal. By lowering the communications rate, the receiver can perfectly decode the communications message from the radar-suppressed joint received signal (which consists of the communications signal, thermal noise, and radar residual). The joint radar-communications receiver uses the decoded communications message to reconstruct and remove the communications waveform from the received signal to obtain a radar return signal free of communications interference. This method of interference cancelation is called SIC. SIC is the same optimal multiuser detection technique used for a two-user multiple-access communications channel [7], [33], except it is now reformulated for a communications and radar user instead of two communications users. The block diagram of the joint radar-communications system considered in this scenario is shown in Fig. 2. For a joint radar-communications received signal, $z(t)$, given by

$$z(t) = b\sqrt{P_{\text{com}}}\,r(t) + n(t) + \sqrt{P_{\text{rad}}}\,a\,x(t-\tau)$$

the received signal at the communications receiver with the predicted radar return suppressed, $\tilde{z}(t)$, is given by [3], [5]

$$\begin{aligned}\tilde{z}(t) &= b\sqrt{P_{\text{com}}}\,r(t) + n(t) \\ &\quad + \sqrt{P_{\text{rad}}}\,a[x(t-\tau) - x(t-\tau_{\text{pre}})] \end{aligned} \tag{1}$$

where $x(t-\tau_{\text{pre}})$ is the predicted radar return signal, and τ_{pre} is the predicted target delay. When applying SIC, the interference residual plus noise signal $n_{\text{int+n}}(t)$, from the communications receiver's perspective, is given by [3], [5]

$$\begin{aligned} n_{\text{int+n}}(t) &= n(t) + n_{\text{resi}}(t) \\ &= n(t) + \sqrt{\|a\|^2\,P_{\text{rad}}}\,n_{\tau,\text{proc}}(t)\,\frac{\partial x(t-\tau)}{\partial t} \end{aligned} \tag{2}$$

where $n_{\tau,\text{proc}}(t)$ is the process noise with variance $\sigma^2_{\tau,\text{proc}}$.

It should be noted that SIC performance is highly sensitive to model mismatch errors since they introduce larger residuals in the SIC process, negatively impacting interference cancelation performance. Potential sources for model mismatch include dynamic range constraints on the receiver or transmitter, phase noise, etc. Insufficient transmitter or

receiver dynamic range implies that if one received signal is stronger than the other signal, mitigating the stronger signal through SIC will be incredibly difficult, resulting in high residual values being present in the weaker signal after SIC. Communications signal mitigation by 40–50 dB has been demonstrated experimentally [34], [35]. As a result, a dynamic range of 50 dB is sufficient to avoid model mismatch errors for the joint radar-communications receiver. Additionally, it should be noted that the performance of the SIC receiver has a complex dependency on receiver phase noise. Large phase noise can introduce larger postradar suppression residual values, negatively impacting joint radar-communications performance. A better analysis of the relationship between the SIC receiver and phase noise can be found in [36].

B. Spectral Water-Filling SIC Data Rate

We develop and present the novel spectral water-filling SIC data rate, which utilizes the continuous spectral water-filling algorithm [7], [37] to determine the optimal communications power distribution over frequency. The continuous spectral water-filling algorithm optimizes the data rate for a given noise power spectral density [7], [37]. Once the receiver model is known, the communications transmitter can easily determine the noise spectral density at the receiver, $N_{\text{int+n}}(f)$, and apply the continuous spectral water-filling algorithm to determine the optimal communications transmit power distribution, $P(f)$. This communications power distribution, $P(f)$, maximizes the communications data rate at which the joint radar-communications receiver decodes the communications message. We define this maximized communications rate as the spectral water-filling SIC data rate. We use the spectral water-filling SIC data rate to measure communications performance. The continuous spectral water-filling algorithm is a continuous form extension of the water-filling algorithm employed in [3] and [5]. Fig. 3 highlights how the continuous spectral water-filling algorithm selects the optimal power distribution.

As mentioned earlier, since we employ the SIC model at the joint radar-communications receiver, the receiver will decode the communications message after the predicted radar signal has been mitigated from the received signal. As a result, from the communications receiver's perspective, the channel will be corrupted by noise given by (2). In order to find the noise spectral density, $N_{\text{int+n}}(f)$, we first calculate the autocorrelation function of the time- and band-limited noise signal, $n(t)$ (since the received signal is also time- and band-limited)

$$\begin{aligned}\gamma(\alpha) &= \left\langle n_{\text{int+n}}(t)\, n^*_{\text{int+n}}(t-\alpha)\right\rangle \\ &= \left\langle n(t)\, n^*(t-\alpha)\right\rangle + \left\langle n_{\text{resi}}(t)\, n_{\text{resi}}(t-\alpha)\right\rangle \\ &= k_B\, T_{\text{temp}}\, B\ \text{sinc}(\pi\ B\,\alpha) \\ &\quad + \|a\|^2\, P_{\text{rad}}\, \sigma^2_{\tau,\text{proc}}\, \frac{\partial x(t-\tau)}{\partial t}\, \frac{\partial x^*(t-\tau-\alpha)}{\partial t}\end{aligned}$$

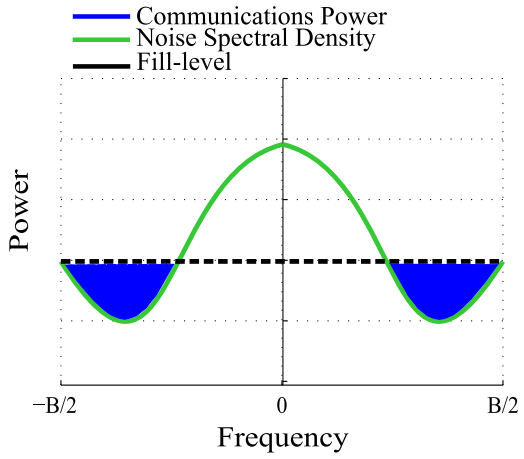

Fig. 3. Notional example of the continuous spectral water-filling algorithm. The black, dashed line indicates the fill level (maximum amount of communications power that can be allocated at any frequency), the green curve represents the noise power spectral density $N_{\text{int+n}}(f)$, and the optimal communications power spectral distribution is shown in blue.

$$\begin{aligned}&= k_B\, T_{\text{temp}}\, B\ \text{sinc}(\pi\ B\,\alpha) + (4\pi^2)\, \|a\|^2\, P_{\text{rad}}\, \sigma^2_{\tau,\text{proc}} \\ &\quad \cdot \int_{-\infty}^{\infty} df f^2 X(f) X^*(f) \mathrm{e}^{i2\pi f\alpha} \\ &= k_B\, T_{\text{temp}}\, B\ \text{sinc}(\pi\ B\,\alpha) \\ &\quad + (4\pi^2)\, \|a\|^2\, P_{\text{rad}}\, \sigma^2_{\tau,\text{proc}}\, g(\alpha) \qquad (3)\end{aligned}$$

where Parseval's theorem and the time-shift and time derivative properties of the Fourier transform are used between the second and third steps, $\text{sinc}(x) = \frac{\sin(x)}{x}$, and $g(\alpha)$ is the inverse Fourier transform with respect to α of $G(f) = \|X(f)\|^2 f^2$. Since the noise power spectral density and autocorrelation are Fourier transform pairs, the noise power spectral density is given by

$$\begin{aligned}N_{\text{int+n}}(f) &= N(f) + N_{\text{resi}}(f) \\ &= k_B\, T_{\text{temp}}\, \Pi_B(f) \\ &\quad + (4\pi^2)\, \|a\|^2\, P_{\text{rad}}\, \sigma^2_{\tau,\text{proc}}\, \|X(f)\|^2\, f^2 \qquad (4)\end{aligned}$$

where $N(f)$ and $N_{\text{resi}}(f)$ are the Fourier transforms of $n(t)$ and $n_{\text{resi}}(t)$, respectively, and $\Pi_B(f)$ is a top-hat or rectangular function from $\frac{-B}{2}$ to $\frac{B}{2}$. The optimal communications power spectrum determined by the continuous spectral water-filling algorithm is given by

$$P(f) = \left(\mu - \frac{N_{\text{int+n}}(f)}{b^2}\right)^+ \qquad (5)$$

where $(x)^+ = x$ if $x \geq 0$; otherwise $(x)^+ = 0$ and μ is a constant that is determined from the power constraint

$$P_{\text{com}} = \int_{\frac{-B}{2}}^{\frac{B}{2}} df\, P(f) = \int_{\frac{-B}{2}}^{\frac{B}{2}} df\, \left(\mu - \frac{N_{\text{int+n}}(f)}{b^2}\right)^+. \qquad (6)$$

The spectral water-filling SIC data rate (the corresponding data rate for the channel with noise spectral density

$N_{\text{int+n}}(f)$) is given by [7], [37]

$$R_{\text{com}} = \int_{\frac{-B}{2}}^{\frac{B}{2}} df \log\left(1 + \frac{b^2\, P(f)}{N_{\text{int+n}}(f)}\right). \tag{7}$$

It should be noted that due to the complexity involved in determining analytical solutions for the integrals shown in (6) and (7), these integrals are evaluated numerically to determine the optimal value for μ and the communications data rate.

C. Global Estimation Rate

Here, we provide a brief discussion of the global estimation rate, which was first developed in [6]. We measure radar performance by the estimation rate [3], [5], which measures the amount of information contained in radar returns. The estimation rate is upper bounded as follows:

$$R_{\text{est}} \leq \frac{\delta}{2T} \log_2\left[1 + \frac{\sigma^2_{\tau,\text{proc}}}{\sigma^2_{\text{est}}}\right] \tag{8}$$

where σ^2_{est} is the range estimation noise variance, which is bounded locally by the Cramer–Rao lower bound (CRLB) [38]. The estimation rate was extended in [6] to account for global estimation errors. The method of interval errors [33], [39], [40] is employed to calculate the effect of nonlocal errors on time-delay estimation performance. A closed-form solution of the probability of side-lobe confusion, $P_{\text{s.l.}}$ is obtained in terms of the values and locations of the side-lobe peaks, integrated radar SNR, and the Marcum Q-function Q_M [33]. The method of intervals time-delay estimation variance is then given by

$$\sigma^2_{\text{est}} = [1 - P_{\text{s.l.}}(\text{ISNR})]\, \sigma^2_{\text{CRLB}}(\text{ISNR}) + P_{\text{s.l.}}(\text{ISNR})\, \phi^2_{\text{s.l.}} \tag{9}$$

where $\phi_{\text{s.l.}}$ is the offset in time (seconds) between the autocorrelation peak side-lobe and main-lobe [5]. The probability of side-lobe confusion, $P_{\text{s.l.}}$, is given by [33]

$$\begin{aligned} P_{\text{s.l.}}(\text{ISNR}) = 1 &- Q_M\left(\sqrt{\frac{\text{ISNR}}{2}\left(1 + \sqrt{1 - \|\rho\|^2}\right)}\right. \\ &\left.\sqrt{\frac{\text{ISNR}}{2}\left(1 - \sqrt{1 - \|\rho\|^2}\right)}\right) \\ &+ Q_M\left(\sqrt{\frac{\text{ISNR}}{2}\left(1 - \sqrt{1 - \|\rho\|^2}\right)}\right. \\ &\left.\sqrt{\frac{\text{ISNR}}{2}\left(1 + \sqrt{1 - \|\rho\|^2}\right)}\right) \end{aligned} \tag{10}$$

where ρ is the ratio of the main-lobe to the peak side-lobe of the autocorrelation function. For a radar system performing time-delay estimation, the CRLB for time delay estimation is given by [41]

$$\sigma^2_{\text{CRLB}} = (8\pi^2 B^2_{\text{rms}} \text{ISNR})^{-1} \tag{11}$$

where the rms bandwidth is given by

$$B^2_{\text{rms}} = \frac{\int f^2 \|X(f)\|^2\, df}{\int \|X(f)\|^2\, df}. \tag{12}$$

A more intuitive understanding of how the estimation rate metric captures target parameter estimation performance and the implications of altering the estimation rate can be found in [4]. The estimation rate is extended to account for Doppler measurement and continuous signaling radars in [42].

III. NONLINEAR CHIRP WITH PARAMETRIC POLYNOMIAL PHASE

In this section, we briefly introduce the novel parameterized nonlinear chirp that will be used to design the optimal radar waveform in the minimum estimation error variance waveform design method. We also derive an approximate closed-form solution for the spectrum for a special case of this nonlinear chirp waveform.

One desirable property for radar waveforms is to have a PAPR as close as possible to 1 (the smallest possible value). Thus, most current radar systems require the signal to be constant modulus or unimodular. This keeps the peak and the average power the same over any time period, granting the signal the smallest possible PAPR of 1. To ensure that the optimized radar waveform is unimodular, we begin by considering the following unimodular nonlinear chirp signal with a polynomial phase

$$x(t) = \mathrm{e}^{i\pi\left(\sum_{m=1}^{N} p_m t^{2m}\right)} \tag{13}$$

where N is a positive integer and $p_m \in \mathbb{R}, \forall m$ are phase coefficients. Note that we have constrained the phase polynomial to have only even-powered terms to ensure symmetry in the frequency domain. The shape of the waveform spectrum is determined by the phase coefficients. The minimum estimation error variance method selects the appropriate phase coefficient values so as to optimize the shape of the radar spectrum to maximize joint radar-communications performance.

In the following discussion, we derive an approximate expression for the spectrum of the nonlinear chirp waveform shown in (13) for $N = 2$.

A. Spectrum of Nonlinear Chirp With Parametric Polynomial Phase

Due to the increased complexity involved in evaluating the spectrum for higher values of N, we consider the simple case of $N = 2$. The spectrum of the band-limited nonlinear chirp with bandwidth B and time-duration T is given by

$$\begin{aligned} X(f) &= \int_{\frac{-T}{2}}^{\frac{T}{2}} dt\, \mathrm{e}^{i\pi(p_1 B^2 t^2 + p_2 B^4 t^4)}\, \mathrm{e}^{-i2\pi f t} \\ &= \int_{\frac{-T}{2}}^{\frac{T}{2}} dt\, \mathrm{e}^{i\pi(p_1 B^2 t^2 + p_2 B^4 t^4 - 2 f t)} \\ &= \int_{\frac{-T}{2}}^{\frac{T}{2}} dt\, \mathrm{e}^{i\phi(t,f)}. \end{aligned} \tag{14}$$

In order to obtain a closed-form solution for the above integral, we employ the principle of stationary phase (PSP) [43]. We first find the points in time, t_0, where the phase, $\phi(t,\, f)$, is stationary, i.e., when

$$\begin{aligned}&\frac{\partial \phi(t,\, f)}{\partial t}\Big|_{t=t_0} = 0\\ &\Rightarrow \pi(2\, p_1\, B^2\, t_0 + 4\, p_2\, B^4\, t_0^3 - 2\, f) = 0\\ &\Rightarrow 2\, p_1\, B^2\, t_0 + 4\, p_2\, B^4\, t_0^3 - 2\, f = 0. \end{aligned} \tag{15}$$

Solving for t_0, we get

$$\begin{aligned} t_0 = {} & \frac{-6^{\frac{2}{3}}\, B^6\, p_1\, p_2}{Q}\\ & + \frac{6^{\frac{1}{3}}\,(9\, B^8\, p_2^2\, f + \sqrt{3\, B^{16}\, p_2^3\,(2\, B^2\, p_1^3 + 27\, p_2\, f^2)})^{\frac{2}{3}}}{Q} \end{aligned} \tag{16}$$

where

$$\begin{aligned} Q = {} & 6\, B^4\, p_2 \Big(9 B^8\, p_2^2\, f\\ & + \sqrt{3\, B^{16}\, p_2^3\,(2\, B^2\, p_1^3 + 27\, p_2\, f^2)}\Big)^{\frac{1}{3}}. \end{aligned}$$

Using the PSP, the expression for an approximation of the spectrum is given by [43]

$$\begin{aligned} X(f) &\approx 2\sqrt{\frac{-\pi}{2\,\phi''(t_0,\, f)}}\, \mathrm{e}^{-i\frac{\pi}{4}}\, x(t_0)\, \mathrm{e}^{i\phi(t_0,\, f)}\\ &= 2\sqrt{\frac{-1}{4\, p_1\, B^2 + 24\, p_2\, B^4\, t_0^2}}\, \mathrm{e}^{-i\frac{\pi}{4}}\, \mathrm{e}^{i\pi(p_1\, B^2\, t_0^2 + p_2\, B^4\, t_0^4)}\\ &\quad \cdot \mathrm{e}^{i\pi(p_1\, B^2\, t_0^2 + p_2\, B^4\, t_0^4 - 2\, f\, t_0)} \end{aligned} \tag{17}$$

where $\phi''(t,\, f) = \frac{\partial^2 \phi(t,\, f)}{\partial t^2} = \pi(2\, p_1\, B^2 + 12\, p_2\, B^4\, t^2)$. The closed form shown in (17) is given for reference and illustration. Its performance is not considered for numerical analysis in the paper.

IV. RADAR WAVEFORM DESIGN METHODS

In this section, we present two radar waveform design algorithms for a joint radar-communications system. We first briefly discuss the spectral mask shaping method that was first introduced in [6]. A novel radar waveform design method, the minimum estimation error variance method, is then presented in this section. The spectral mask shaping method will be used as a baseline to compare the performance of the minimum estimation error variance method presented in this paper.

A. Spectral Mask Shaping Method

We present the radar waveform design method presented in [6]. This method will be used as a performance baseline to compare the performance of the novel radar waveform design method presented in this paper. The radar waveform can be designed to maximize radar estimation rate, communications rate, or some weighting therein. Without consideration of global error, waveform design can be simplified to tuning B_{rms} [3]. A closed-form, parameterized spectral mask is used to tune B_{rms} to jointly maximize both the radar and communications users' information rate.

We assume we have a linear FM chirp, which spans from $-B/2$ to $B/2$ in time T. We then apply a frequency-domain spectral mask weighting to the chirp, $W(f) = x + z\, f^2,\, |f| \leq \frac{B}{2}$. The rms bandwidth of the resulting weighted chirp is found by assuming that the chirp spectrum is approximately flat using the PSP [43]. As a result, the rms bandwidth is easily calculable in closed form for the polynomial [6]

$$B_{\text{rms}} = \sqrt{\frac{\frac{x^2\, B^3}{12} + \frac{x\, z\, B^5}{40} + \frac{z^2\, B^7}{448}}{x^2\, B + \frac{x\, z\, B^3}{6} + \frac{z^2\, B^5}{80}}}. \tag{18}$$

Using differential evolution [44] to tune B_{rms}, the following objective function (or cost function) is optimized to maximize joint performance (radar and communications users' information rate)

$$R_{\text{total}} = R_{\text{est}}(B_{\text{rms}})^{\alpha}\, \tilde{R}_{\text{com}}(B_{\text{rms}})^{(1-\alpha)} \tag{19}$$

where $\tilde{R}_{\text{com}}(B_{\text{rms}})$ is the SIC communications data rate defined in [3] (not to be confused with the spectral water-filling SIC data rate defined in this paper) and α is a blending parameter that is varied from 0 to 1. When $\alpha = 0$, only communications rate is considered. When $\alpha = 1$, only the radar estimation rate is considered. In between, the product is jointly maximized. Note that for $\alpha = 0.5$, R_{total} represents the geometric mean of the two rates. This provides a more numerically stable error term, even when $\tilde{R}_{\text{com}} \gg R_{\text{est}}$.

B. Minimum Estimation Error Variance Method

The waveform design algorithm that we propose in this section designs an optimal nonlinear chirp radar waveform (as modeled in Section III) from a global estimation rate perspective. In other words, we first design the waveform to minimize the global estimation error variance (estimation error variance taking into account both nonlocal and local estimation errors), given by (9). This minimization of the global estimation error variance is accomplished by minimizing the estimation error variance at the radar threshold SNR of the radar estimator. The threshold point of an estimator is the estimator (or radar) SNR value at which the estimator's performance deviates from the CRLB [38] due to error contributions from nonlocal estimation errors. At SNR values lower than the threshold point, due to autocorrelation main-lobe–side-lobe confusion, nonlocal estimation errors begin to contribute to estimator's error variance, which causes the estimation performance to degrade and deviate from the CRLB [33]. Since the threshold point is the SNR point at which an estimator's performance deviates from the CRLB and also the SNR point at which nonlocal estimation errors contribute to estimation performance, minimizing the CRLB at the threshold point gives the lowest possible global estimation error variance or highest possible global estimation rate.

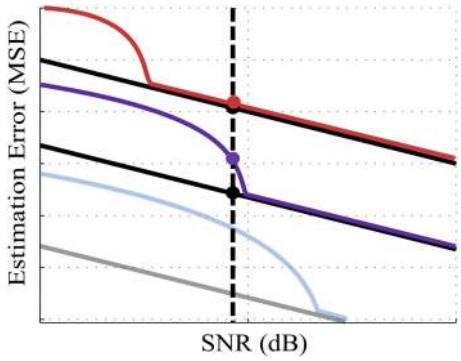

Fig. 4. Notional example depicting the impact of the constraint given by (20) on the feasible set for optimization. The dashed vertical line indicates the given signal-to-noise ratio (SNR). The red, purple and blue solid curves indicate the estimator performance for different radar waveforms and the black solid lines indicate the Cramér-Rao lower bound (CRLB) for each radar waveform. The black dots indicate the CRLB values for various feasible radar waveforms at the given SNR. The red and purple dots indicate the actual estimation error variance (estimation performance) for various feasible radar waveforms at the given SNR. The grayed out curves indicate estimation performance for unfeasible radar waveforms at the given SNR. Minimizing the CRLB over the feasible set ensures that the optimal radar waveform will have the lowest estimation threshold point (or best estimation performance, taking both local and non-local estimation errors).

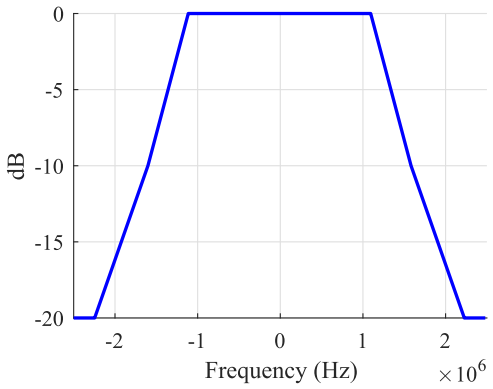

Fig. 5. Spectral leakage mask used constrain the amount of energy in the radar spectrum leaking out at frequencies out of the system bandwidth range. The spectral leakage constraint is enforced by having the radar spectrum be below this thresholding spectral leakage mask.

For a given SNR, we have to design a radar waveform that has a threshold point at that SNR and has the best (or smallest) estimation error variance. We first eliminate all radar waveforms that have a threshold point higher than the current SNR and then, from the remaining feasible solution set, we find the radar waveform that minimizes the CRLB given by (11). We perform the first elimination step by imposing the following constraint on the ratio of the global estimation error variance [given by (9)] and the CRLB [given by (11)]

$$\frac{\sigma^2_{\text{est}}}{\sigma^2_{\text{CRLB}}} \leq \delta_{\text{constraint}} \tag{20}$$

where $\delta_{\text{constraint}}$ is a parameter whose value determines the size of the feasible solution set. We discuss how to tune this parameter in Section V. By ensuring the above ratio stays below $\delta_{\text{constraint}}$, any radar waveforms with higher threshold points (SNR values) are eliminated. Fig. 4 depicts how this constraint works on eliminating radar waveforms with higher threshold points.

We also introduce an additional constraint on spectral leakage (constraint $\boldsymbol{C_2}$) to the waveform optimization problem in order to obtain optimal radar waveforms that not only ensure optimal joint radar-communications performance, but also satisfy additional real-world properties that a traditional radar waveform would. Since the system can only receive signals whose spectrum lies within the system's bandwidth, any RF energy that leaks outside of the bandwidth will be lost. To minimize this loss of RF energy, we introduce a constraint on the amount of energy present in the radar spectrum at frequencies out of the system bandwidth range. We enforce this spectral leakage constraint by having the radar spectrum be below a thresholding spectral mask such as the one seen in Fig. 5.

We consider the nonlinear chirp waveform given by (13). The spectral shape of the waveform is determined by the parameters $p_m, m = 1, \ldots, N$. In order to design the radar waveform spectrum that minimizes the global estimation performance, we solve the following optimization problem:

$$\begin{aligned} \underset{\bar{p}}{\text{minimize}} \quad & \frac{1}{8\pi^2 B_{\text{rms}}(\bar{p})^2 T B(\text{SNR})}, \\ \text{subject to} \quad & p_m \in [0, 10] \quad \forall m \\ & \frac{\sigma^2_{\text{est}}}{\sigma^2_{\text{CRLB}}} \leq \delta_{\text{constraint}} \\ & \mathbb{1}_A(\bar{p}) = 1 \qquad (\boldsymbol{C_2}) \end{aligned} \tag{21}$$

where $\bar{p} = (p_1, \ldots, p_N)$, and $p_1, \ldots, p_N$ are the coefficients of the phase polynomial for the unimodular waveform in (13), and $B_{\text{rms}}(\bar{p})$ is given by (12). The constraint $\boldsymbol{C_2}$ constrains the coefficients $\bar{p}$ such that the resulting spectrum of the waveform stays below a certain masking threshold, which is represented by an indicator function, where A is the set of all phase coefficients that let the resulting masked spectrum stay below the masking threshold as shown in Fig. 5.

Once the optimal radar waveform that maximizes the radar performance of a joint radar-communications system is designed, the continuous spectral water-filling algorithm described in Section II-B is employed to determine the spectral water-filling SIC data rate that maximizes the communications performance of a joint radar-communications system. This optimization process is called the minimum estimation error variance method. It should be noted that the optimization problem described in (21) is a nonconvex optimization problem.

C. Impact of Threshold Point SNR

As mentioned in Section I, we saw from [3] and [5] that the spectral shape of the radar waveform (the radar rms bandwidth) impacts the performance of a joint

radar-communications system. Shaping the radar spectrum imposes a tradeoff both in terms of radar performance versus communications performance and in terms of improved estimation performance versus an increased radar threshold SNR. In this section, we briefly discuss how the choice of the threshold SNR impacts both the shape of the radar waveform spectrum and the performance of the joint radar-communications system.

Selecting a low value for the threshold SNR implies that even for small radar SNR values, the probability of side-lobe confusion for the radar waveform autocorrelation function (which causes the estimator performance to deviate from the CRLB) is small. Radar waveforms with more energy at frequencies closer to center of the bandwidth allocation can have such autocorrelation functions. However, such a radar waveform has a smaller rms bandwidth, which degrades the overall estimation performance as seen in (11). Furthermore, as we observed from (4), radar waveforms with more spectral energy at the bandwidth center will reduce the noise spectral density, $N_{\text{int+n}}(f)$, due to minimal radar residual values ($N_{\text{resi}}(f)$), thereby maximizing the data rate.

Conversely, selecting a larger value for the threshold point implies that there is more ambiguity in the radar waveform autocorrelation function (higher side-lobes), which occurs for radar waveforms with more energy at frequencies closer to the edges of the bandwidth allocation. Such waveforms also have larger rms bandwidth values and a better estimation performance. Finally, radar waveforms with more spectral energy at the bandwidth edges have larger $N_{\text{resi}}(f)$ values and consequently, larger $N_{\text{int+n}}(f)$ values, which degrade the communications data rate.

Thus, we see that selecting a low radar SNR threshold point increases the communications performance and decreases the radar performance but also results in a radar waveform with low side-lobes in the autocorrelation. Similarly, selecting a high threshold point increases the radar performance and decreases the communications performance but also results in a radar waveform with large autocorrelation side-lobes. The objective is to select a threshold point that optimizes the spectral shape of the radar waveform such that the performance with respect to radar and communications is jointly maximized.

The results from the numerical study of the above optimization problem are discussed in Section V.

V. SIMULATION RESULTS

In this section, we present an example of the waveform design technique discussed in this paper, the minimum estimation error variance method, for an example parameter set. The parameters used in the example are shown in Table II. Additionally, a performance comparison of the minimum estimation error variance method with the previously derived spectral mask shaping method is also provided. We also study the effect of the order of the nonlinear chirp phase on joint radar-communications performance. In order to better solve the nonconvex optimization problem described in Section IV-B, all the results presented below were obtained by solving the optimization problem in (21) using *fmincon* [45] for 100 Monte-Carlo runs with randomized initial solutions and selecting the solution with the highest objective value.

TABLE II
Parameters For Waveform Design Methods

Parameter	Value
Bandwidth (B)	5 MHz
Center Frequency	3 GHz
Effective Temperature (T_{temp})	1000 K
Communications Range	10 km
Communications Power (P_{com})	45 W
Communications Antenna Gain	0 dBi
Communications Receiver Side-lobe Gain	10 dBi
Radar Target Range	200 km
Radar Antenna Gain	30 dBi
Target Cross Section	10 m^2
Target Process Standard Deviation ($\sigma_{\tau,\text{proc}}$)	100 m
Time-Bandwidth Product (TB)	128
Radar Duty Factor (δ)	0.01
Threshold Point Constraint ($\delta_{\text{constraint}}$)	$1 + 0.01$

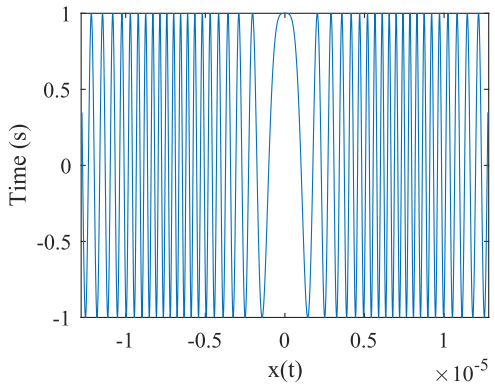

Fig. 6. Real valued amplitude of waveform versus time (s). We see that the radar waveform has a chip shape similar to a nonlinear chirp in the time domain. The constant modulus nature of the radar waveform is also clearly evident.

A. Minimum Estimation Error Variance Method Optimal Waveform Shape

Here we present an example of a joint radar-communications optimal radar waveform designed by the minimum estimation error variance method. Figs. 6 and 7 show time-domain and time-frequency representations of the nonlinear chirp waveform with a phase polynomial shown in (13) for the number of phase polynomial coefficients, $N = 6$ and a threshold SNR value of 0 dB. Fig. 6 shows the real valued amplitude of the waveform as a function of time. We see that the radar waveform has a chip shape similar to a nonlinear chirp in the time domain. The constant modulus nature of the radar waveform is also apparent from the figure. Fig. 7 shows the short-time Fourier transform spectrogram as a function of time and frequency. From this figure, we observe that the optimal radar waveform has a nonlinear time-frequency representation and is similar to a sum of polynomials.

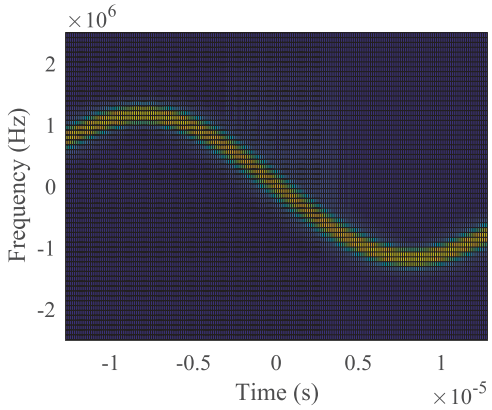

Fig. 7. Short-time Fourier transform spectrogram versus time (s) and frequency (Hz). We observe that the optimal radar waveform has a non-linear time-frequency representation and is similar to a sum of polynomials.

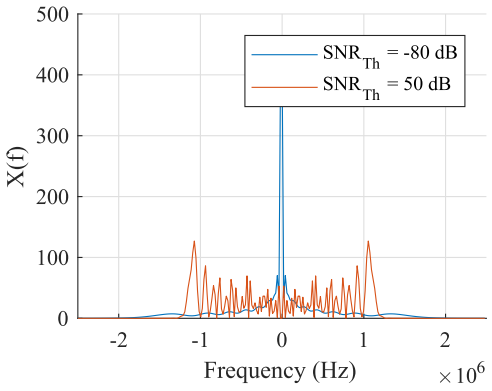

Fig. 8. Minimum estimation error variance optimized radar waveform spectrum for different threshold SNR values. The radar waveform optimization was done for $N = 6$. We see the optimal radar spectrum has more spectral energy at the edges of the bandwidth for high threshold SNR values and has more spectral energy closer to the center for low threshold SNR values.

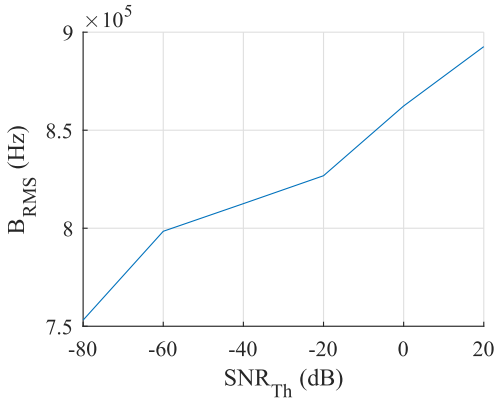

Fig. 9. Rms bandwidth of the optimized radar waveform versus SNR. As expected, the optimal rms bandwidth increases as we increase the threshold SNR. From (11), we see that the optimal rms bandwidth increasing as the threshold SNR increases will thereby reduce the CRLB. As a result, we see that the estimation performance increases with SNR.

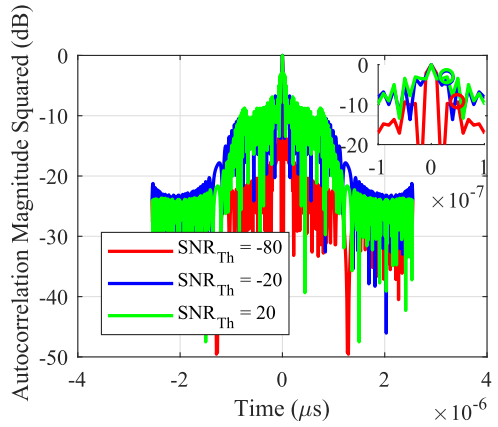

Fig. 10. Autocorrelation function of the optimized radar waveform versus SNR. As expected, the peak side-lobe of the autocorrelation function increases as we increase the threshold SNR. This trend is observed because a higher threshold SNR implies the optimal waveform has more ambiguity, which translates into higher peak autocorrelation side-lobes.

B. Impact of Threshold SNR

We now discuss the numerical results from implementing the minimum estimation error variance method in Section IV-B. First, we highlight the impact of the threshold SNR value on the shape of the radar spectrum. We consider two threshold SNR values of -80 and 50 dB and we choose $N = 6$ in (13), i.e., $x(t) = e^{i\pi(\sum_{m=1}^{6} p_m t^{2m})}$. The minimum estimation error variance optimized radar waveform spectrum for this set of parameters is shown in Fig. 8. From Fig. 8, we see the optimal radar spectrum has more spectral energy at the edges of the bandwidth for high threshold SNR values and has more spectral energy closer to the center for low threshold SNR values, as we stated in Section IV-C.

We also study the impact of the threshold SNR (or radar SNR) on the system performance. For the purpose of this study, we choose $N = 6$. For different values of SNR, we optimize the shape of the waveform, i.e., optimize the coefficients $\bar{p} = (p_1, \ldots, p_6)$, to minimize the CRLB achieved with the waveform. We also impose the constraint $\sigma^2_{\text{est}}/\sigma^2_{\text{CRLB}} \leq \delta_{\text{constraint}}$, which ensures that for the given SNR, our feasible solution set include only waveforms whose threshold SNR is less than or equal to the given SNR (as discussed in Section IV-B). $\delta_{\text{constraint}}$ is tuned so that the ratio between the estimation error variance (which characterizes estimation performance in this paper) and the CRLB remains close to 1. For this simulation, we consider a $\delta_{\text{constraint}}$ value of $1 + \epsilon$, where ϵ introduces some flexibility to the constraint and typically has a value of 0.01.

Fig. 9 shows the rms bandwidth values achieved with each optimized waveform for various values of threshold SNR. As expected, the optimal rms bandwidth increases as we increase the threshold SNR. From (11) and Section IV-C, we see that the optimal rms bandwidth increasing as the threshold SNR increases will thereby reduce the CRLB as stated in Section IV-C.

Fig. 10 shows the autocorrelation function achieved with each optimized waveform for various values of threshold SNR. For SNR values -80, -20, and 20 dB, we observed that the peak side-lobes in all three cases occur at

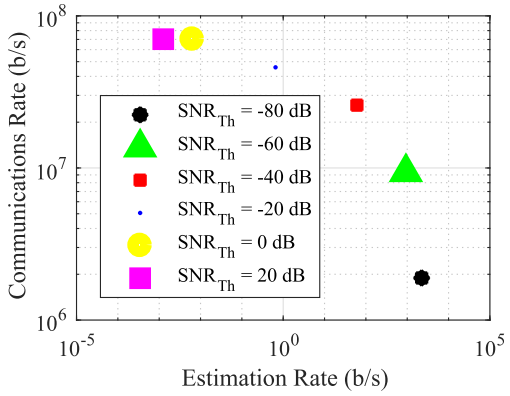

Fig. 11. Estimation and data rates versus threshold SNR. Clearly, we see the performance of the system improve with respect to the estimation rate and degrade with respect to the spectral water-filling successive interference cancellation (SIC) data rate as we increase the threshold SNR.

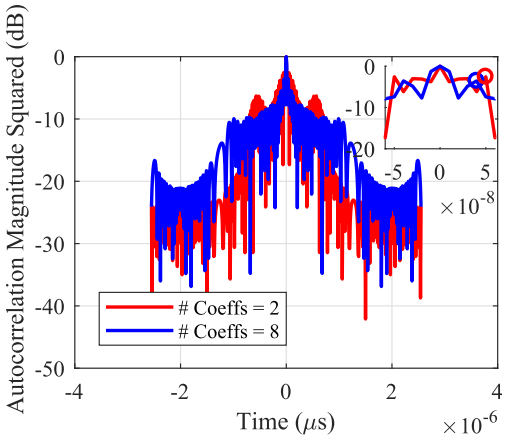

Fig. 12. Autocorrelation function of the optimized radar waveform versus N. We clearly see that the autocorrelation peak side-lobes decrease as N increases, which causes the estimation performance to improve overall as N increases.

± 0.2–0.5 μs and have values of -10, -7, and -6 dB, respectively. As expected, the peak side-lobe of the autocorrelation function increases as we increase the threshold SNR. As mentioned in Section IV-C, a higher threshold SNR implies that the optimal waveform has more ambiguity, which translates to higher peak autocorrelation side-lobes.

Now, for each threshold SNR value considered and for each optimal waveform shape parameter vector $(p_1, p_2, p_3, p_4, p_5, p_6)$ obtained above, we evaluate the radar estimation rate bound in (8) and the spectral water-filling SIC data rate in (7) corresponding to each of these waveforms. Fig. 11 shows the plot of estimation rate and the data rate against the threshold SNR value. According to the figure, the performance of the system improves with respect to the estimation rate as we increase the threshold SNR, which is expected as the minimum achievable CRLB decreases with threshold SNR, and the estimation rate increases with decreasing CRLB according to (8) and (9). However, we observe that the spectral water-filling SIC data rate reduces as the threshold SNR increases. This trend occurs because, as we stated in Section IV-C, as the threshold SNR increases, the noise spectral density, $N_{\text{int+n}}(f)$ achieves higher values due to larger radar residual values, which reduces the spectral water-filling SIC data rate.

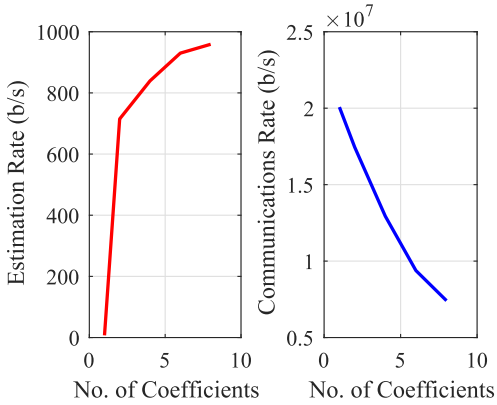

Fig. 13. Estimation and data rates versus N. We see that as N increases, the estimation rate increases and the spectral water-filling SIC data rate decreases. The improvement in estimation rates as N increases is because there are more degrees of freedom available to shape the optimal radar waveform spectrum, which results in optimal waveforms that have better or lower autocorrelation side-lobe levels. Additionally, increasing N means increasing the amount of energy at higher frequencies for the radar waveform spectrum, which improves local estimation performance. Furthermore, the increase in the radar waveform's spectral content at higher frequencies, due to an increase in N, means that the noise spectral density, $N_{\text{int+n}}(f)$, achieves higher values due to larger radar residual values, which reduces the spectral water-filling SIC data rate.

C. Impact of Order of Chirp Phase

We first investigate the relationship between the autocorrelation peak side-lobe levels and the order of the nonlinear chirp waveform's phase, N. Fig. 12 shows the autocorrelation function for $N = 2$ and $N = 8$ at a threshold SNR value of 0 dB. We clearly see that the autocorrelation peak side-lobes decrease as N increases, which causes the estimation performance to improve overall as N increases.

As the shape of the waveform explicitly depends on the coefficients $p_1, \ldots, p_N$ in (21), we now study the effect of the number of coefficients, N, on both the estimation and the data rates. For this study, we choose a threshold SNR value of 0 dB and vary N from 1 to 8. For each N and threshold SNR value, we solve (21) and evaluate the estimation rate from (8) and spectral water-filling SIC data rate from (7). Fig. 13 shows plots of these rates against N. From Fig. 13, we see that as N increases, the estimation rate increases and the spectral water-filling SIC data rate decreases. The improvement in estimation rates as N increases is because there are more degrees of freedom available to shape the optimal radar waveform spectrum obtained by solving the optimization problem in (21). As a result of these increased degrees of freedom, optimal radar waveforms are obtained that have better or lower autocorrelation side-lobe levels (a trend we observed earlier). Additionally, increasing N means increasing the amount of energy at higher frequencies for the radar waveform spectrum, which results in the

TABLE III
Minimum Estimation Error Versus Spectral-Mask Shaping For SNR = 7.6 dB

Performance metric (average values)	Min. Est. Error	Spectral-Mask Shaping
R_{est} (b/s)	1.38×10^3	1.06×10^3
R_{com} (b/s)	6.92×10^6	1.38×10^4

B_{rms} value increasing, there by improving local estimation performance given by (11). This increase in local estimation performance, coupled with lower autocorrelation sidelobe levels, results in an overall increase in the estimation rate as N increases. Furthermore, the increase in the radar waveform's spectral content at higher frequencies, due to an increase in N, means that the noise spectral density, $N_{int+n}(f)$, achieves higher values due to larger radar residual values, which reduces the spectral water-filling SIC data rate.

D. Performance Comparison of Waveform Design Algorithms

We compare the performance of the minimum estimation error variance method against the spectral mask shaping method in [6]. We conduct a Monte Carlo study with 50 runs to compare the performance of these methods. For this study, we choose the SNR of 7.6 dB, and set $N = 6$. In each Monte Carlo run, we evaluate the estimation rates and the communications rates (spectral water-filling SIC data rate for the minimum estimation error variance method and the SIC data rate for the spectral mask shaping method) from the two methods. Table III shows the average of estimation rates (R_{est}) and communications rates (R_{com}) from the Monte-Carlo study.

From Table III, we clearly observe that the minimum estimation error variance method outperforms the spectral-mask shaping method in terms of estimation rate and communications rate. Furthermore, a significant increase in the achieved communications rate highlights the impact of the continuous water-filling algorithm. Thus, we see the explicit advantage of the proposed method over the method in [6] in that the minimum estimation error variance method proposed in this paper designs radar waveforms that are constant modulus and ensures better estimation performance and better communications performance over the spectral shaping method.

VI. CONCLUSION

We presented a novel radar waveform design technique that maximizes the performance of a spectrum sharing, joint radar-communications system. The global estimation rate, an extension on the estimation rate that takes into account nonlocal or global estimation errors, and the data rate are used to measure radar and communications performance, respectively. We developed the novel minimum estimation error variance radar waveform design method that selects the phase parameters of a nonlinear chirp radar waveform to maximize radar performance. We also developed the spectral water-filling SIC data rate, which is the maximized communications data rate for a joint radar-communications receiver employing SIC. This data rate was obtained by employing the continuous spectral water-filling algorithm, which determines the optimal communications power spectral distribution for a given noise spectral density. We presented examples of the minimum estimation error variance radar waveform design method for an example parameter set and also compared the method's performance against the performance of the previously derived spectral mask shaping method. We saw that the minimum estimation error variance method is able to achieve higher estimation and communications data rate values than the spectral mask shaping method. We also observed that the optimal estimation rate increases for higher radar SNR values whereas the optimal spectral-water-filling SIC data rate decreases for higher radar SNR values. Finally, we observed that the estimation rate increases and the spectral water-filling SIC data rate decreases as the number of coefficients in the phase of the nonlinear chirp increases.

ACKNOWLEDGMENT

Any opinions, findings, and conclusions or recommendations expressed in this material are those of the authors and do not necessarily reflect the views of the Office of Naval Research or the U.S. Government.

REFERENCES

[1] B. Paul, A. R. Chiriyath, and D. W. Bliss
Survey of RF communications and sensing convergence research
IEEE Access, vol. 5, pp. 252–270, 2016.

[2] H. Griffiths *et al.*
Radar spectrum engineering and management: Technical and regulatory issues
Proc. IEEE, vol. 103, no. 1, pp. 85–102, Jan. 2015.

[3] D. W. Bliss
Cooperative radar and communications signaling: The estimation and information theory odd couple
In *Proc. IEEE Radar Conf.*, May 2014, pp. 50–55.

[4] A. R. Chiriyath, B. Paul, and D. W. Bliss
Radar-communications convergence: coexistence, cooperation, and co-design
IEEE Trans. Cogn. Commun. Netw., vol. 3, no. 1, pp. 1–12, Feb. 2017.

[5] A. R. Chiriyath, B. Paul, G. M. Jacyna, and D. W. Bliss
Inner bounds on performance of radar and communications coexistence
IEEE Trans. Signal Process., vol. 64, no. 2, pp. 464–474, Jan. 2016.

[6] B. Paul, A. R. Chiriyath, and D. W. Bliss
Joint communications and radar performance bounds under continuous waveform optimization: The waveform awakens
In *Proc. IEEE Radar Conf.*, May 2016, pp. 865–870.

[7] T. M. Cover and J. A. Thomas
Elements of Information Theory, 2nd ed. Hoboken, NJ, USA: Wiley, 2006.

[8] B. Paul and D. W. Bliss
The constant information radar
Entropy, vol. 18, no. 9, 2016, Art. no. 338. [Online]. Available: http://www.mdpi.com/1099-4300/18/9/338

[9] A. R. Chiriyath, B. Paul, and D. W. Bliss
Simultaneous radar detection and communications performance with clutter mitigation
In *Proc. IEEE Radar Conf.*, May 2017, pp. 279–284.

[10] C. Sturm and W. Wiesbeck
Waveform design and signal processing aspects for fusion of wireless communications and radar sensing
Proc. IEEE, vol. 99, no. 7, pp. 1236–1259, Jul. 2011.

[11] A. Turlapaty, Y. Jin, and Y. Xu
Range and velocity estimation of radar targets by weighted OFDM modulation
In *Proc. IEEE Radar Conf.*, May 2014, pp. 1358–1362.

[12] T. Guo and R. Qiu
OFDM waveform design compromising spectral nulling, sidelobe suppression and range resolution
In *Proc. IEEE Radar Conf.*, May 2014, pp. 1424–1429.

[13] G. Lellouch, A. Mishra, and M. Inggs
Impact of the Doppler modulation on the range and Doppler processing in OFDM radar
In *Proc. IEEE Radar Conf.*, May 2014, pp. 803–808.

[14] S. C. Thompson and J. P. Stralka
Constant envelope OFDM for power-efficient radar and data communications
In *Proc. Int. Waveform Diversity Design Conf.*, Feb. 2009, pp. 291–295.

[15] X. Shaojian, C. Bing, and Z. Ping
Radar-communication integration based on DSSS techniques
In *Proc. 8th Int. Conf. Signal Process.*, Nov. 2006, vol. 4, pp. 1–4.

[16] Y. Xie, R. Tao, and T. Wang
Method of waveform design for radar and communication integrated system based on CSS
In *Proc. 1st Int. Conf. Instrum., Meas., Comput., Commun. Control*, Oct. 2011, pp. 737–739.

[17] M. Roberton and E. R. Brown
Integrated radar and communications based on chirped spread-spectrum techniques
In *Proc. IEEE MTT-S Int. Microw. Symp. Digest*, Jun. 2003, vol. 1, pp. 611–614.

[18] A. Khawar, A. Abdel-Hadi, and T. C. Clancy
MIMO radar waveform design for coexistence with cellular systems
In *Proc. IEEE Int. Symp. Dyn. Spectrum Access Netw.*, Apr. 2014, pp. 20–26.

[19] Y. L. Sit and T. Zwick
MIMO OFDM radar with communication and interference cancellation features
In *Proc. IEEE Radar Conf.*, May 2014, pp. 265–268.

[20] B. Li, A. P. Petropulu, and W. Trappe
Optimum co-design for spectrum sharing between matrix completion based MIMO radars and a MIMO communication system
IEEE Trans. Signal Process., vol. 64, no. 17, pp. 4562–4575, May 2016.

[21] Y. Zhang, Q. Li, L. Huang, and J. Song
Waveform design for joint radar-communication system with multi-user based on MIMO radar
In *Proc. IEEE Radar Conf.*, May 2017, pp. 0415–0418.

[22] A. Aubry, V. Carotenuto, A. De Maio, A. Farina, and L. Pallotta
Optimization theory-based radar waveform design for spectrally dense environments
IEEE Aerosp. Electron. Syst. Mag., vol. 31, no. 12, pp. 14–25, Dec. 2016.

[23] Y. Huang, M. Piezzo, V. Carotenuto, and A. De Maio
Radar waveform design under similarity, bandwidth priority, and spectral coexistence constraints
In *Proc. IEEE Radar Conf.*, May 2017, pp. 1142–1147.

[24] A. Aubry, V. Carotenuto, and A. De Maio
Radar waveform design with multiple spectral compatibility constraints
In *Proc. IEEE Radar Conf.*, May 2016, pp. 1–6.

[25] J. Qian, M. Lops, L. Zheng, X. Wang, and Z. He
Joint system design for coexistence of MIMO radar and MIMO communication
IEEE Trans. Signal Process., vol. 66, no. 13, pp. 3504–3519, Jul. 2018.

[26] A. Khawar, A. Abdel-Hadi, and T. C. Clancy
Spectrum sharing between S-band radar and LTE cellular system: A spatial approach
In *Proc. IEEE Int. Symp. Dyn. Spectrum Access Netw.*, Apr. 2014, pp. 7–14.

[27] S. Sodagari, A. Khawar, T. C. Clancy, and R. McGwier
A projection based approach for radar and telecommunication systems coexistence
In *Proc. IEEE Global Commun. Conf.*, Dec. 2012, pp. 5010–5014.

[28] H. Shajaiah, A. Abdelhadi, and C. Clancy
Spectrum sharing approach between radar and communication systems and its impact on radars detectable target parameters
In *Proc. IEEE 81st Veh. Technol. Conf.*, May 2015, pp. 1–6.

[29] W. Zhang, S. Vedantam, and U. Mitra
Joint transmission and state estimation: A constrained channel coding approach
IEEE Trans. Inf. Theory, vol. 57, no. 10, pp. 7084–7095, Oct. 2011.

[30] P. Stinco, M. Greco, F. Gini, and B. Himed
Channel parameters estimation for cognitive radar systems
In *Proc. 4th Int. Workshop Cogn. Inf. Process.*, May 2014, pp. 1–6.

[31] A. Pezeshki, A. R. Calderbank, W. Moran, and S. D. Howard
Doppler resilient Golay complementary waveforms
IEEE Trans. Inf. Theory, vol. 54, no. 9, pp. 4254–4266, Sep. 2008.

[32] B. Li and A. Petropulu
MIMO radar and communication spectrum sharing with clutter mitigation
In *Proc. IEEE Radar Conf.*, May 2016, pp. 1–6.

[33] D. W. Bliss and S. Govindasamy
Adaptive Wireless Communications: MIMO Channels and Networks. New York, NY, USA: Cambridge Univ. Press, 2013.

[34] A. Sabharwal, P. Schniter, D. Guo, D. W. Bliss, S. Rangarajan, and R. Wichman
In-band full-duplex wireless: Challenges and opportunities
IEEE J. Sel. Areas Commun., vol. 32, no. 9, pp. 1637–1652, Sep. 2014.

[35] D. W. Bliss, P. A. Parker, and A. R. Margetts
Simultaneous transmission and reception for improved wireless network performance
In *Proc. IEEE/SP 14th Workshop Statist. Signal Process.*, Aug. 2007, pp. 478–482.

[36] A. R. Chiriyath, B. Paul, and D. W. Bliss
Joint radar-communications information bounds with clutter: The phase noise menace
In *Proc. IEEE Radar Conf.*, May 2016, pp. 690–695.

[37] R. G. Gallager
Information Theory and Reliable Communication, 2nd ed. Hoboken, NJ, USA: Wiley, 1968.

[38] S. M. Kay
Fundamentals of Statistical Signal Processing: Estimation Theory, 1st ed. Upper Saddle River, NJ, USA: Prentice-Hall, 1993.

[39] C. D. Richmond
Mean-squared error and threshold SNR prediction of maximum-likelihood signal parameter estimation with estimated colored noise covariances
IEEE Trans. Inf. Theory, vol. 52, no. 5, pp. 2146–2164, May 2006.

[40] H. Van Trees
Detection, Estimation, and Modulation Theory: Part 1, 1st ed. Hoboken, NJ, USA: Wiley, 2004.

[41] M. A. Richards
Principles of Modern Radar: Basic Principles, J. A. Sheer and W. A. Holm Eds. Raleigh, NC, USA: SciTech Publishing, 2010.

[42] B. Paul and D. W. Bliss
Extending joint radar-communications bounds for FMCW radar with Doppler estimation
In *Proc. IEEE Radar Conf.*, May 2015, pp. 89–94.

[43] M. A. Richards
Fundamentals of Radar Signal Processing, 2nd ed. Raleigh, NC, USA: McGraw-Hill, 2013.

[44] S. Das and P. N. Suganthan
Differential evolution: A survey of the state-of-the-art
IEEE Trans. Evol. Comput., vol. 15, no. 1, pp. 4–31, Feb. 2011.

[45] MATLAB's *fmincon*. 2016. [Online]. Available: https://www.mathworks.com/help/optim/ug/fmincon.html?requestedDomain=ww w.mathworks.com

Alex Rajan Chiriyath (S'16–M'18) received the B.S.E.E. degree (*Cum Laude*) in electrical engineering from the University of Michigan at Ann Arbor, Ann Arbor, MI, USA, in 2012 and the M.S. degree and Ph.D. degree in electrical engineering from Arizona State University, Tempe, AZ, USA, in 2014 and 2018.

He is currently a Postdoctoral Researcher with BLISS Labs and WISCA with Arizona State University. His main research interest includes RF convergence between radar and communications systems.

Shankarachary Ragi (S'11–M'16) received the Bachelor's and Master's degrees in electrical engineering from Indian Institute of Technology Madras, Chennai, India, in 2009. He received the Doctoral degree in electrical and computer engineering from Colorado State University, Fort Collins, CO, USA, in 2014.

After briefly working in industry post Ph.D., he joined the Department of Mathematics, Arizona State University in 2016 as a Postdoctoral Research Associate. He is currently an Assistant Professor with the Department of Electrical and Computer Engineering, South Dakota School of Mines and Technology, Rapid City, SD, USA. His research interests include autonomous unmanned systems and swarm intelligence, and deal with various aspects such as optimal decision making, motion planning, sensor fusion, and swarm tactics.

Dr. Ragi is an Associate Editor for IEEE ACCESS.

Hans D. Mittelmann received the M.S. degree in mathematics from the University of Mainz, Mainz, Germany, in 1971, and the Ph.D. degree and the Habilitation degree in mathematics from the Technical University in Darmstadt, Darmstadt, Germany, in 1973 and 1976, respectively.

He was an Associate Professor with the University of Dortmund, Dortmund, Germany, in 1977. In 1982, he became a full Professor with Arizona State University. His current research interest includes computational optimization and its applications.

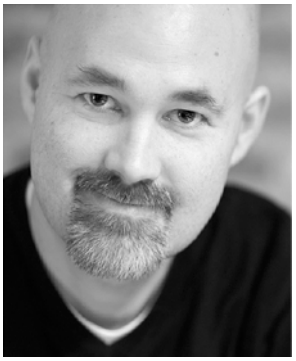

Daniel W. Bliss (F'15) received the B.S.E.E. degree in electrical engineering from Arizona State University, Tempe, AZ, USA, in 1989, the M.S. degree in physics, and the Ph.D. degree from the University of California at San Diego, La Jolla, CA, USA in 1995 and 1997, respectively.

Employed by General Dynamics from 1989 to 1993, he designed rocket avionics and performed magnetic field calculations and optimization for high-energy particle-accelerator superconducting magnets. His doctoral work (1993–1997) was in the area of high-energy particle physics. He was a Senior Member of the technical staff with MIT Lincoln Laboratory from 1997 to 2012. He is currently an Associate Professor with the School of Electrical, Computer and Energy Engineering, Arizona State University. His current research topics include multiple-input multiple-output (MIMO) wireless communications, MIMO radar, cognitive radios, radio network performance, geolocation, and statistical signal processing for anticipatory physiological analytics. He has been the Principal Investigator on numerous programs with applications to radio, radar, and medical monitoring. He has made significant contributions to robust multiple-antenna communications including theory, patents, and the development of advanced prototypes. He is responsible for some of the foundational MIMO radar literature.